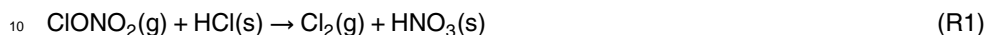


1997). PSC's are classified according to their composition, consisting either of crystalline NAT (type Ia), ternary $\text{H}_2\text{SO}_4/\text{HNO}_3/\text{H}_2\text{O}$ supercooled solution (type Ib) or pure H_2O ice (type II) (Zondlo et al., 2000).

Heterogeneous reactions occurring on PSC's convert the major unreactive chlorine reservoir compounds, ClONO_2 and HCl , into molecular chlorine, which is rapidly photolyzed into atomic chlorine. Reaction (R1) is the most important chlorine-activating reaction in the polar stratosphere because it converts two moles of unreactive chlorine compounds into two moles of atomic chlorine after photolysis in an efficient heterogeneous reaction (Seinfeld and Pandis, 2006):



Reaction (R1) belongs to one of the fastest stratospheric reactions (Friedl et al., 1986; Molina et al., 1985, 1987), orders of magnitude faster than the corresponding homogeneous gas phase process (Molina et al., 1985). The Cl_2 released in the gas phase from Reaction (R1) rapidly photolyzes into free Cl atoms which then establish a rapid cycle of O_3 destruction. Furthermore, Reaction (R1) also leads to the overall removal of nitrogen oxides from the gas phase, trapping HNO_3 in the ice and thus facilitating O_3 destruction through a catalytic cycle as reported in Reactions (R2)–(R4):



where X is H, OH, NO, Cl or Br leading to HO_x , NO_x , ClO_x and BrO_x catalytic cycles, respectively.

The understanding of the interaction of HCl with ice is crucial in order to determine the availability of HCl at the gas-ice condensed phase interface for Reaction (R1) to effectively happen. To this purpose, the HCl/ice system has been extensively studied over the years by means of different techniques. Laminar flow tubes and Knudsen

30767

reactors are among the most widely used devices when coupled with diagnostic techniques such as ellipsometry (McNeill et al., 2006), Fourier Transform Infrared (FTIR) spectroscopy in transmission (Ritzhaupt and Devlin, 1991; Koehler et al., 1993; Delzeit et al., 1993) and Reflection-Absorption Infrared Spectroscopy (RAIRS) (Banham et al., 1996; Graham and Roberts, 1997). Two crystalline hydrates have been found at temperatures that may be relevant for the upper troposphere and lower stratosphere, the hexahydrate ($\text{HCl} \cdot 6\text{H}_2\text{O}$) and the trihydrate ($\text{HCl} \cdot 3\text{H}_2\text{O}$). Moreover, amorphous mixtures of variable $\text{H}_2\text{O} : \text{HCl}$ ratios, may well be relevant at stratospheric conditions.

The phase diagram of the HCl/ H_2O system constructed by Molina and coworkers (Molina, 1994; Wooldridge et al., 1995) indicates that the HCl trihydrate requires HCl concentrations much higher than found in the stratosphere ($[\text{HCl}] = 1\text{--}3$ ppb, Carslaw et al., 1997) and therefore has no atmospheric relevance. On the other hand, HCl hexahydrate may nucleate at HCl concentrations of atmospheric relevance but at temperatures lower than normally found during polar nights such that its atmospheric relevance has been questioned as well (Koehler et al., 1993; McNeill et al., 2007; Chiesa and Rossi, 2013). It thus appears that only amorphous HCl/ H_2O mixtures have atmospheric relevance which are in addition more reactive than the crystalline phase $\text{HCl} \cdot 6\text{H}_2\text{O}$ as far as Reaction (R1) is concerned (McNeill et al., 2006, 2007).

In this study we focused our attention on the HCl hexahydrate phase as well as on amorphous mixtures of concentrations comparable to HCl hexahydrate in order to compare its behaviour under typical stratospheric conditions of $[\text{H}_2\text{O}] = 2\text{--}6$ ppm and $[\text{HCl}] = 1\text{--}3$ ppb (Carslaw et al., 1997). Our results are in agreement with previous studies in showing that the irreversible conversion of HCl hexahydrate into an amorphous 6 : 1 $\text{H}_2\text{O} : \text{HCl}$ mixture occurred at temperatures higher than 190 K (Graham and Roberts, 1997; Sadtchenko et al., 2000; Chiesa and Rossi, 2013) and that the amorphous HCl/ H_2O phase had a higher reactivity compared to the crystalline $\text{HCl} \cdot 6\text{H}_2\text{O}$ under similar HCl and H_2O vapour pressures (McNeill et al., 2006; Chiesa and Rossi, 2013).

30768

8×10^{-6} Torr at SFR conditions and under simultaneous monitoring of HCl at $m/z = 36$. A total dose of approximately 5×10^{17} molecules of HCl is admitted into the reactor. It is important to notice that not all the admitted HCl molecules are adsorbed onto the ice film as roughly 50 % of them are lost either through pumping across the effusion orifice or by adsorption onto the chamber walls. The mass balance for a few selected experiments will be displayed below. The formation of HH on the ice sample is monitored by means of FTIR absorption spectroscopy in transmission as a function of time, both during deposition of HCl and once the admission of HCl has been halted.

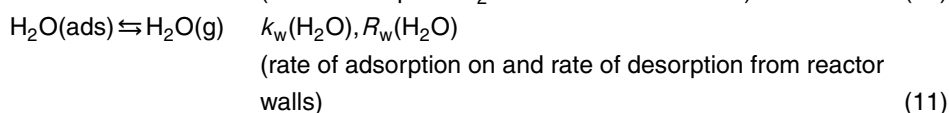
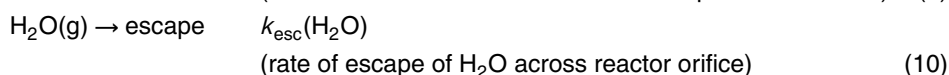
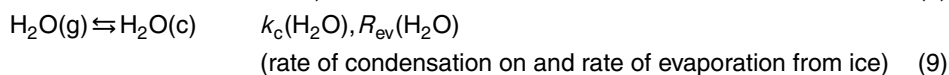
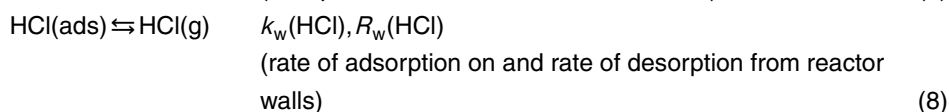
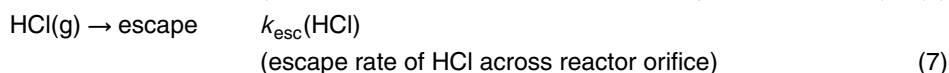
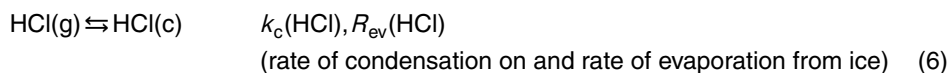
The protocol for the growth of amHCl films differs from the HH growth protocol only in the choice of temperature at which the sample is exposed to HCl. After the growth of the pure ice film, the temperature is increased to 175–178 K when a similar dose of HCl compared to HH growth is admitted into the reactor and monitored at $m/z = 36$ (HCl) and $m/z = 18$ (H_2O). Similarly, the formation of amHCl on the thin ice film sample is monitored using FTIR absorption spectroscopy.

3 Experimental methodology

The stirred-flow reactor is characterized by a large internal surface compared to the Si substrate surface (Table 1). Due to the small ratio between these surfaces it is inevitable that atmospheric trace gases admitted during the experiments interact with the stainless steel chamber walls. In order to describe the interaction of H_2O and HCl vapour with the low temperature ice films and the chamber walls the following scheme

30775

has been applied:



where $k_c(\text{HCl})$, $k_c(\text{H}_2\text{O})$ are the condensation rate constants on ice in s^{-1} for HCl and H_2O , $R_{\text{ev}}(\text{HCl})$, $R_{\text{ev}}(\text{H}_2\text{O})$ the evaporation rates from the ice in $\text{molec s}^{-1} \text{cm}^{-3}$, $k_w(\text{HCl})$, $k_w(\text{H}_2\text{O})$ the adsorption rate constants onto the reactor walls, $R_w(\text{HCl})$, $R_w(\text{H}_2\text{O})$ the desorption rates from the walls in $\text{molec s}^{-1} \text{cm}^{-3}$ and $k_{\text{esc}}(\text{HCl})$, $k_{\text{esc}}(\text{H}_2\text{O})$ the effusion rate constants out of the reactor in s^{-1} , respectively.

The aim of this study is to separate the rate of evaporation R_{ev} and the accommodation coefficient α on ice for both gases, HCl and H_2O , in order to obtain the kinetics of evaporation and condensation. Both kinetic parameters are subsequently combined to obtain the corresponding HCl and H_2O equilibrium vapour pressures that may be compared to literature measurements. This approach is known as thermo-chemical ki-

30776

The dashed green line represents extrapolated values of $P_{\text{eq}}(\text{H}_2\text{O})$ for temperatures lower than 173 K.

The values obtained for the equilibrium vapour pressure have been compared with the HCl/H₂O phase diagram constructed by Molina and coworkers (Abbatt, 1992; Molina, 1994; Wooldridge, 1995). Figure 7 shows the results for amHCl films, which all lie within the existence area of HH. This is expected since the dose admitted into the reactor chamber is the same used during the HH growth protocol, namely 5×10^{17} molecules of HCl compared to approximately 4×10^{18} molecules of H₂O, corresponding to an average mole fraction $\chi_{\text{HCl}} = 0.111$.

4.2 Crystalline hexahydrate films

The results for HH are reported in Fig. 8. Panel c shows the measured $\alpha_{\text{ice}}(X)$ as a function of temperature. Inverse blue triangles represent $\alpha_{\text{ice}}(\text{H}_2\text{O})$ on pure ice, as shown in Fig. 6. $\alpha_{\text{ice}}(\text{H}_2\text{O})$ on HH (red circles) decreases a function of temperature and is lower by a factor of approximately 1.5 than $\alpha_{\text{ice}}(\text{H}_2\text{O})$ on pure ice at temperatures higher than 185 K. Coloured triangles represent results for $\alpha_{\text{ice}}(\text{HCl})$ on HH, with the colour scale showing the increasing accumulated dose of HCl on the HCl-doped ice film. $\alpha_{\text{ice}}(\text{HCl})$ shows larger scatter compared to amHCl with a variation up to a factor of 10 for results at the same temperature across the full temperature range. Furthermore, each series of three pulses spaced by typically 60 to 90 s always showed a decrease in $\alpha_{\text{ice}}(\text{HCl})$ between the first and the last pulse. Similar results have been shown previously in the literature (McNeill et al., 2007) where the scatter has been explained in terms of the morphology or the smoothness of the ice surface. We will discuss these results further in the discussion section.

Panel b shows results for the R_{ev} in $\text{molec s}^{-1} \text{cm}^{-3}$ as a function of temperature. $R_{\text{ev}}(\text{HCl})$ on HH, represented by black triangles, is lower by a factor of 100 across the temperature range 165–193 K compared to $R_{\text{ev}}(\text{H}_2\text{O})$ on HH which, being equal to $R_{\text{ev}}(\text{H}_2\text{O})$ on pure ice within experimental error, indicates that the presence of crys-

30787

talline HH on the ice substrate does not substantially affect the evaporation of H₂O which is that of pure ice, in a manner similar to amHCl as described before.

Panel a shows the results for P_{eq} in Torr calculated according to Eq. (22) for both H₂O and HCl. $P_{\text{eq}}(\text{H}_2\text{O})$ of HH is equal to $P_{\text{eq}}(\text{H}_2\text{O})$ of pure ice within experimental error whereas $P_{\text{eq}}(\text{HCl})$ of HH is lower by a factor of 4 to 15 compared to $P_{\text{eq}}(\text{H}_2\text{O})$ of HH. The scatter of $P_{\text{eq}}(\text{HCl})$, being of the same magnitude as the scatter of $\alpha_{\text{ice}}(\text{HCl})$, may likewise be explained by a variation in the substrate composition as well as by an increase in its roughness or inhomogeneous nature due to the exposure to HCl pulses.

Figure 9 shows the phase diagram of the results obtained for HH films: most of the results lie in the HH existence region, as expected, but there is a significant number of points lying outside the HH existence area. In order to determine whether or not this result pertains to the hexahydrate phase we took advantage of the multidagnostic capabilities of the apparatus and focused our attention to the condensed phase using the corresponding FTIR spectrum for each of the experiments in question.

4.3 FTIR spectra of hexahydrate

The FTIR spectrum of hexahydrate is known from the literature (Ritzhaupt and Devlin, 1991; Koehler et al., 1993; Toon et al., 1994; Graham and Roberts, 1997). For each point in Fig. 9, a corresponding spectrum of the thin film has been collected. All spectra corresponding to experiments lying in the HH existence region are a mixture of pure ice and HH film as they have the spectroscopic signature of hexahydrate phase, namely the two additional peaks in the OH stretching region at 3426 and 3366 cm^{-1} and the sharp peak at 1635 cm^{-1} , corresponding to the bending vibration of the proton ordered waters of hydration. Likewise, the spectra corresponding to experiments lying outside the known published HH existence region appear to be a combination of pure ice and pure HH. In order to clearly indicate the presence of HH as well as the HH : ice mixing ratio for these experiments we deconvoluted all experimental spectra. We assume that the measured composite spectrum is a superposition of the spectra of pure ice and pure HH, and we proceeded as follows in order to deconvolute the absorption spec-

30788

trum: the sharp IR peak at 1635 cm^{-1} is an unambiguous marker of HH. Therefore, the optical density at this peak can be used as a marker of the amount of HH present in the ice film. We scaled the optical density at 1635 cm^{-1} of an independently recorded spectrum of pure HH to that of the spectrum of interest. The scaled spectrum is that
5 of the pure HH component and we obtain the pure ice component from the measured composite spectrum after subtraction.

Figure 10 shows an example of the deconvolution: the green spectrum is the recorded spectrum, that is the superposition of pure HH and pure H_2O -ice, the red spectrum is the measured spectrum of pure HH scaled to the measured amplitude of
10 the IR absorption peak at 1635 cm^{-1} and the blue spectrum corresponds to the difference of the green and the red spectrum. It is obvious that the measured spectrum is that of a film where pure ice and pure HH coexist. The procedure does not take into account possible small shifts of up to $\pm 2\text{ cm}^{-1}$ of the pure component spectrum in the presence of the other component, in agreement with the wavelength accuracy of the
15 FTIR spectrometer in the current configuration.

Figure 11 shows the HCl/ H_2O phase diagram and the FTIR spectra of a few experiments outside the known HH existence area, labelled accordingly. Each spectrum panel shows the measured FTIR spectrum in the same colour as the vapour pressure
20 plotted in the bottom left panel as well as its deconvolution into a pure ice component (blue spectrum) and a pure HH component (red spectrum). This procedure has been applied to all experiments outside the known HH existence area. For all cases the same conclusion has been reached, namely that all measured $P_{\text{eq}}(\text{HCl})$ results in Fig. 9 are indeed pertaining to binary HH/ice films of various composition.

30789

5 Discussion

5.1 Langmuir adsorption isotherms

In order to describe the adsorption of HCl and H_2O onto the reactor internal surface we used Langmuir adsorption isotherms to fit the experimental measurements of HCl
5 and H_2O surface coverage. As shown in Fig. 4, the presence of a HCl flow during H_2O steady state experiments (green circles) presumably enhances the capability of H_2O to adsorb onto the walls, whereas the presence of an additional H_2O flow during HCl exposure reduces the HCl coverage. This may be due to the fact that H_2O and HCl are adsorbed onto different adsorption sites in single gas experiments, but in the presence
10 of a HCl flow the H_2O may also adsorb onto HCl occupied sites, perhaps owing to the high solubility of HCl in H_2O at large H_2O surface coverage. The system, on the other hand, is not symmetric and HCl may be more site-selective compared to H_2O . Therefore, the presence of an additional H_2O flow reduces the number of available sites for HCl adsorption and thus the internal wall coverage of HCl.

15 Another reason for the decrease of HCl coverage in the presence of H_2O may be the so called common ion effect, induced by the presence of two NaCl salt windows of 20 cm^2 surface ($2''$ diameter): the sodium chloride on the salt windows is dissociated by water into Na^+ and Cl^- ions. The common Cl^- ion reduces the solubility of HCl thus limiting the coverage on the walls. This effect may help reduce the coverage of HCl, but
20 due to the limited surface of the NaCl windows (40 cm^2) compared to the total internal surface (1885 cm^2) it is unlikely to explain the reduction of K_L by approximately a factor of 7 shown in Fig. 4.

Langmuir isotherms are not the only isotherms used to describe surface adsorption. For instance, Deitz and Turner (1970) used conventional Type II physical adsorption
25 isotherms to describe the adsorption of water on the walls of a glass-Kovar stainless steel vacuum system in the pressure range from 0.2 to 5 Torr. They conclude that the water adsorption strongly depends on the materials and needs to be determined for each apparatus. On the other hand, electrochemical quartz crystal measurements have

30790

Table 3 shows results for all experiments reported performed. In all cases the mass balance ratio and the stoichiometry of the condensed phase have been calculated at the end of the HH growth protocol, once steady state conditions had been reached and before PV experiments began. The mass balance ratio yields an average value of 1.182 ± 0.123 . The wall-adsorbed molecules account for about 12 to 19% of the total number of molecules let into the reactor and for about 22 to 30% of the number of molecules adsorbed onto the ice. These results show that particular caution has to be paid to the description of the gas-wall interaction in the SFR due to the importance it has in the processes involved. The calculated stoichiometry yields an average value of 5.82 ± 0.79 , comparable to the theoretical value of 6 for $\text{HCl} \cdot 6\text{H}_2\text{O}$. If we regard experiment 4 as an outlier because it is barely inside the 2σ interval, we obtain an average value for the stoichiometry of the crystalline phase of 6.16 ± 0.29 , remarkably close to the expected theoretical value considering the experimental uncertainty.

5.3 HCl/H₂O phase diagram

As described in Sect. 4.3, the deconvolution procedure shown in Fig. 11 leads to observable HCl hexahydrate concentrations for all experiments conducted outside the known HH existence area. They all pertain to binary HH/ice films and we, therefore, propose to extend the existence area of $\text{HCl} \cdot 6\text{H}_2\text{O}$ by modifying the HCl/H₂O phase diagram to include the present results, as shown in Fig. 12 by the shaded area. We preserve the slope of the coexistence line of hexahydrate and trihydrate as calculated by Wooldridge et al. (1995) and simply apply a parallel displacement of the phase boundary whose slope depends on the stoichiometry of the two hydrates and their enthalpies of sublimation.

Figure 13a shows the phase diagram as a function of the equilibrium vapour pressures $P_{\text{eq}}(\text{H}_2\text{O})$ and $P_{\text{eq}}(\text{HCl})$, reconstructed from Hanson and Mauersberger (1990). The empty triangles represent the calculated values of $P_{\text{eq}}(\text{H}_2\text{O})$ and $P_{\text{eq}}(\text{HCl})$ for HH using the kinetic results for adsorption and desorption obtained from the present work, according to Eq. (22). The proposed extension of the HH existence area is represented

30793

as well. The quadruple points remain and are not affected by the additional data. Figure 13b shows an example of two experiments as a time-series when the temperature of the ice substrate is increased in the range 167 to 197 K. Both experiments have been performed as described in Sect. 3.3.

Before describing the two experiments represented by red and purple lines, it is important to understand the behaviour of a sample in a simpler case. We will follow the black dotted line labelled “180 K” in panel a, which represents the isotherm at temperature $T = 180\text{ K}$. Along this line, $P_{\text{eq}}(\text{HCl})$ may be increased up to approximately 2.5×10^{-7} Torr with almost no detectable change in $P_{\text{eq}}(\text{H}_2\text{O})$. The sample behaves as pure ice even in the presence of small amounts of HCl. When the phase boundary line is reached, the phase changes from “ice” to HH. Any further increase of $P_{\text{eq}}(\text{HCl})$ corresponds to a decrease of $P_{\text{eq}}(\text{H}_2\text{O})$ as expected for a binary system at equilibrium following the law of Gibbs–Duhem, Eq. (25):

$$d\mu_{\text{HCl}} = -\frac{n_{\text{H}_2\text{O}}}{n_{\text{HCl}}} \cdot d\mu_{\text{H}_2\text{O}} \quad (25)$$

where n_{HCl} and $n_{\text{H}_2\text{O}}$ are the number of moles of HCl and H₂O and $d\mu_{\text{HCl}}$ and $d\mu_{\text{H}_2\text{O}}$ the change in chemical potential, respectively. A variation in the chemical potential of a component (HCl) in the condensed phase corresponds to the inverse variation of the chemical potential of the other component (H₂O) in proportion to the stoichiometric ratio of the two components. A large variation of $P_{\text{eq}}(\text{HCl})$ is allowed along an isotherm compared to a much smaller variation of $P_{\text{eq}}(\text{H}_2\text{O})$.

As HCl increases along the isotherm, $P_{\text{eq}}(\text{H}_2\text{O})$ decreases until the boundary line between hexahydrate and trihydrate is reached and the phase changes again. The slope is less steep, reflecting the change of stoichiometry in the new solid phase. A change in temperature leads to deviations from this simple case and the substrate may follow different paths to reach equilibrium. The experiments shown as red and purple lines in panel b describe the evolution of the substrate when the partial pressure of water is controlled by the introduction of an external H₂O flow $F_{\text{in}}(\text{H}_2\text{O})$ into the reactor.

30794

First we will discuss the experiment marked in red symbols in Fig. 13b. Point 1 is the first measurement taken at 171 K, subsequently the temperature is increased to point 2 (175 K) while no external flow of H_2O is introduced. Nevertheless, a substantial decrease in $P_{\text{eq}}(\text{HCl})$ is observed, not only during this particular experiment, but for all experiments reported in panel a. As explained above, a decrease in $P_{\text{eq}}(\text{HCl})$ corresponds to an increase of $P_{\text{eq}}(\text{H}_2\text{O})$, which implies the presence of a flow of H_2O . The water is introduced into the reactor involuntarily across numerous small leaks owing to the presence of elastomeric seals (Viton O-rings) which add up so as to become non-negligible at these low partial pressures of H_2O . Consistent with this fact is our observation of an increase of the thickness of the ice film due to deposition of H_2O onto the ice at temperatures lower than 175 K.

From point 2 to point 3 (180 K) the temperature is increased and only a small increase in $P_{\text{eq}}(\text{H}_2\text{O})$ is observed compared to a large increase of $P_{\text{eq}}(\text{HCl})$. Between point 3 to point 4 $F_{\text{in}}(\text{H}_2\text{O})$ is introduced into the reactor at constant temperature. As a consequence $P_{\text{eq}}(\text{HCl})$ decreases along the isotherm following the increase of $P_{\text{eq}}(\text{H}_2\text{O})$ as expected according to Gibbs–Duhem, Eq. (25). Both the temperature and $F_{\text{in}}(\text{H}_2\text{O})$ are increased from point 4 to point 7 such that $F_{\text{in}}(\text{H}_2\text{O})$ is kept approximately at $0.1 \cdot F_{\text{ev}}(\text{H}_2\text{O})$ at any temperature. After the measurement at point 7, $F_{\text{in}}(\text{H}_2\text{O})$ is halted and the system immediately responds to the variation of $P_{\text{eq}}(\text{H}_2\text{O})$ by increasing $P_{\text{eq}}(\text{HCl})$ following the isotherm at $T = 190\text{K}$, according to Gibbs–Duhem, Eq. (25).

The experiment marked in purple symbols in Fig. 13b is performed in a similar way as above (red symbols) with the difference that the external flow $F_{\text{in}}(\text{H}_2\text{O})$ is a factor of 2 lower with respect to the “red” experiment. From point 1 to point 2 we observe a drop in $P_{\text{eq}}(\text{HCl})$ due to background H_2O flow and at point 6 $F_{\text{in}}(\text{H}_2\text{O})$ is introduced into the reactor. A lower $F_{\text{in}}(\text{H}_2\text{O})$ leads to higher $P_{\text{eq}}(\text{HCl})$ compared to the “red” experiment as is evident from points 7, 8 and 9 that explore the hitherto unexplored space of the HCl hexahydrate phase diagram marked as shaded area in Fig. 13. At point 10 the flow $F_{\text{in}}(\text{H}_2\text{O})$ is increased to approximately $0.2 \cdot F_{\text{ev}}(\text{H}_2\text{O})$ with a corresponding increase

30795

of $P_{\text{eq}}(\text{H}_2\text{O})$ and decrease of $P_{\text{eq}}(\text{HCl})$ along the isotherm, once again according to Gibbs–Duhem, Eq. (25).

5.4 $\alpha(\text{HCl})$ scatter and HCl hexahydrate composition

Figure 8 shows the kinetic results for HH substrate experiments. Variations in the kinetic and thermodynamic parameters up to a factor of 10 for points at the same temperatures occur. The substrate is a binary system composed of a bulk pure ice film with a thinner HH film on top of it. According to Gibbs’ phase rule, we have $F = C - P + 2 = 2 - 3 + 2 = 1$, where F is the number of degrees of freedom, C the number of components, namely H_2O and HCl, and P the number of phases of the system at equilibrium, namely the binary condensate, the pure ice and the gas phase. The degree of freedom of our system corresponds to the composition of the substrate, namely the mole ratio between pure ice and the HH film. Even though the growth protocol has been applied consistently to all experiments, the approach to the temperatures of interest and the exposure to transient supersaturation of gases during PV experiments which all contribute to the “history” of the film, may lead to a different composition of the thin film at the same experimental temperature which may explain, at least in part, the scatter of $\alpha_{\text{ice}}(\text{HCl})$ as a function of temperature. The decrease of $\alpha_{\text{ice}}(\text{HCl})$ in the aftermath of a pulse may also be explained as a variation of the composition of the interface, specifically a variation from a H_2O -rich ice film before the first pulse of HCl to a more H_2O -deficient ice film when the third HCl pulse is admitted due to evaporation of H_2O and accumulation of HCl.

$\alpha_{\text{ice}}(\text{H}_2\text{O})$ on the other hand, does not present any scatter and this may be due to the fact that the average molecular environment for H_2O is constant owing to its single-component nature: H_2O PV experiments always increase the concentration of H_2O in the film, leading to pure ice behaviour.

In order to evaluate the ratio between pure HH and pure H_2O ice we have made use of the multidagnostic capabilities of the present system. We have selected experiments in five temperature ranges, and for each experiment we have determined the number of

30796

Equilibrium is established when $J_{\text{ads,w}} = J_{\text{des}}$

$$\frac{\alpha_w(X) \cdot \bar{c}}{4} (1 - \theta) \cdot [X] = k_{\text{des}} \cdot \theta \cdot N_{\text{MAX}} \quad (\text{A4})$$

which may be expressed in the form of a Langmuir isotherm as

$$\theta = \frac{K_L [X]}{1 + K_L [X]} \quad (\text{A5})$$

5 with the Langmuir constant of partition coefficient K_L ($\text{cm}^3 \text{molec}^{-1}$) given by:

$$K_L = \frac{\alpha_w(X) \cdot \bar{c} / 4}{N_{\text{MAX}} \cdot k_{\text{des,w}}(X)} \quad (\text{A6})$$

The desorption rate constant $k_{\text{des,w}}$ is calculated from Eq. (A6) as:

$$k_{\text{des,w}}(X) = \frac{\alpha_w(X) \cdot \bar{c} / 4}{N_{\text{MAX}} \cdot K_L} \quad (\text{A7})$$

10 with K_L , N_{MAX} and α_w measured for the SRF according to the methods described in Sects. 3.1 and 3.2. The flow balance Eq. (A1) may now be written as follow:

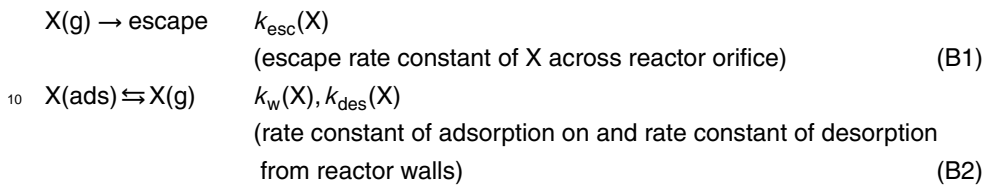
$$\begin{aligned} V \cdot R_{\text{in}}(X) + S_w \cdot N_{\text{MAX}} \cdot k_{\text{des,w}}(X) \cdot \theta + V \cdot R_{\text{ev}}(X) &= \\ = V \cdot R_{\text{SS}}(X) + S_w \cdot \frac{\alpha_w(X) \cdot \bar{c}}{4} (1 - \theta) \cdot [X] + S_{\text{ice}} \cdot \frac{\alpha_{\text{ice}}(X) \cdot \bar{c}}{4} \cdot [X] & \quad (\text{A8}) \end{aligned}$$

15 Substituting $S_w \cdot N_{\text{MAX}} = N_{\text{TOT}}$, the total number of molecules that can be adsorbed onto the total internal surface of the SFR, we may obtain Eq. (13).

30807

Appendix B

In order to describe the temporal evolution of the total number of molecules N in the SFR reactor in the aftermath of a pulse experiment, we will first describe the simpler case with no ice and extend it afterwards to the case in the presence of ice. In the absence of an ice film, the scheme presented in Eqs. (6)–(11), can be simplified as follow for a gas X ($X = \text{HCl}, \text{H}_2\text{O}$):



In the aftermath of a pulse the following rate equation holds:

$$15 \quad \frac{dN}{dt} = F_{\text{des}} - F_{\text{esc}} - F_{\text{ads}} \quad (\text{B3})$$

where all terms are flow rates in molec s^{-1} . N is the total number of molecules inside the reactor, F_{des} the desorption flow rate from the reactor walls, F_{esc} the effusion rate across the orifice and F_{ads} the adsorption flow rate onto the reactor walls, respectively. The number of molecules N may be expressed as $N = [X] \cdot V$, where V is the total volume of the SFR. The flow rates may be given in terms of fluxes as $F_y = J_y \cdot S$, where 20 S is the internal surface of the reactor and J_y is the corresponding flux. According to Eqs. (A2) and (A3), Eq. (B3) may be expressed as:

$$\frac{dN}{dt} = S \cdot k_{\text{des}} \cdot \theta \cdot N_{\text{MAX}} - k_{\text{esc}} \cdot N - S \cdot \frac{\alpha_w \cdot \bar{c}}{4} (1 - \theta) \cdot \frac{N}{V} \quad (\text{B4})$$

30808

- Hanson, D. R. and Ravishankara, R.: Investigation of the reactive and nonreactive processes involving ClONO_2 and HCl on water and nitric acid doped ice, *J. Phys. Chem.*, 96, 2682–2691, 1992.
- Haynes, W. M., Bruno, T. J., and Lide, D. R. (Eds.): Handbook of Chemistry and Physics, 94th edn. (Internet Version 2014), CRC Press/Taylor and Francis, Boca Raton, FL, 2013.
- Henson, B. F., Wilson, K. R., Robinson, J. M., Noble, C. A., Casson, J. L., and Worsnop, D. R.: Experimental isotherms of HCl on H_2O ice under stratospheric conditions: connections between bulk and interfacial thermodynamics, *J. Chem. Phys.*, 121, 8486–8499, 2004.
- Huthwelker, T., Malmström, M. E., Helleis, F., Moortgat, G. K., and Peter, T.: Kinetics of HCl uptake on ice at 190 and 203 K: implications for the microphysics of the uptake process, *J. Phys. Chem. A*, 108, 6302–6318, 2004.
- Hynes, R. G., Mössinger, J. C., and Cox, R. A.: The interaction of HCl with water-ice at tropospheric temperatures, *Geophys. Res. Lett.*, 28, 2827–2830, 2001.
- Koehler, B. G., McNeill, L., Middlebrook, A. M., and Tolbert, M. A.: Fourier transform infrared studies of the interaction of HCl with model polar stratospheric cloud films, *J. Geophys. Res.*, 98, D6, 10563–10571, 1993.
- Marti, J. and Mauersberger, K.: A survey and new measurements of ice vapor pressure at temperatures between 170 and 250 K, *Geophys. Res. Lett.*, 20, 363–366, 1993.
- McNeill, V. F., Loerting, T., Geiger, F. M., Trout, B. L., and Molina, M. J.: Hydrogen chloride-induced surface disordering on ice, *P. Natl. Acad. Sci. USA*, 103, 9422–9427, 2006.
- McNeill, V. F., Geiger, F. M., Loerting, T., Trout, B. L., Molina, L. T., and Molina, M. J.: Interaction of hydrogen chloride with ice surfaces: the effects of grain size, surface roughness and surface disorder, *J. Phys. Chem. A*, 111, 6274–6284, 2007.
- Molina, L. T., Molina, M. J., Stachnik, R. A., and Tom, R. D.: An upper limit to the rate of the HCl + ClONO_2 reaction, *J. Phys. Chem.*, 89, 3779–3781, 1985.
- Molina, M. J.: The probable role of stratospheric “ice” clouds: heterogeneous chemistry of the ozone hole, in: *The Chemistry of the Atmosphere: Its Impact of Global Change*, chapter 3, Blackwell Scientific Publications, London, 27–38, 1994.
- Molina, M. J., Tso, T. L., Molina, L. T., and Wang, F. C. Y.: Antarctic stratospheric chemistry of chlorine nitrate, hydrogen chloride and ice: release of active chlorine, *Science*, 238, 1253–1257, 1987.
- Peter, T.: Microphysics and heterogeneous chemistry of Polar Stratospheric Clouds, *Annu. Rev. Phys. Chem.*, 48, 785–822, 1997.

30815

- Pouvesle, N., Kippenberger, M., Schuster, G., and Crowley, J. N.: The interaction of H_2O_2 with ice surfaces between 203 and 233 K, *Phys. Chem. Chem. Phys.*, 12, 15544–15550, 2010.
- Répánszki, R., Kerner, Z., and Nagy, G.: Adsorption of fission products on stainless steel and zirconium, *Adsorption*, 13, 201–207, 2007.
- Ritzhaupt, G. and Devlin, J. P.: Infrared spectra of nitric and hydrochloric acid hydrate thin films, *J. Phys. Chem.*, 95, 90–95, 1991.
- Sadtchenko, V., Giese, C. F., and Gentry, W. R.: Interaction of hydrogen chloride with thin ice films: the effect of ice morphology and evidence for unique surface species on crystalline vapor-deposited ice, *J. Phys. Chem. B*, 104, 9421–9429, 2000.
- Seinfeld, J. H. and Pandis, S. N.: *Atmospheric Chemistry and Physics: From Air Pollution to Climate Change*, ch. 5, 2nd edn., John Wiley & Sons, 2006.
- Solomon, S., Garcia, R. R., Rowland, F. S., and Wuebbles, D. J.: On the depletion of Antarctic ozone, *Nature*, 321, 755–758, 1986.
- Toon, O. B., Tolbert, M. A., Koehler, B. G., Middlebrook, A. M., and Jordan, J.: Infrared optical constants of H_2O ice, amorphous nitric acid solutions, and nitric acid hydrates, *J. Geophys. Res.*, 99, 631–654, 1994.
- von Hessberg, P., Pouvesle, N., Winkler, A. K., Schuster, G., and Crowley, J. N.: Interaction of formic and acetic acid with ice surfaces between 187 and 117 K. Investigation of single species- and competitive adsorption, *Phys. Chem. Chem. Phys.*, 10, 2345–2355, 2008.
- Wagman, D. D., Evans, W. H., Parker, V. B., Schumm, R. H., Halow, I., Bailey, S. M., Churney, K. L., and Nuttall, R. L.: NBS tables of chemical thermodynamic properties – selected values for inorganic and C_1 and C_2 organic substances in SI units, *J. Phys. Chem. Ref. Data*, 11, Suppl. 2, 1982.
- Winkler, A. K., Holmes, N. S., and Crowley, J. N.: Interaction of methanol, acetone and formaldehyde with ice surfaces between 198 and 223 K, *Phys. Chem. Chem. Phys.*, 4, 5270–5275, 2002.
- Wooldrige, P. J., Zhang, R., and Molina, M. J.: Phase Equilibria of H_2SO_4 , HNO_3 and HCl hydrates and the composition of polar stratospheric clouds, *J. Geophys. Res.*, 100, 1389–1396, 1995.
- Xueref, I. and Dominé, F.: FTIR spectroscopic studies of the simultaneous condensation of HCl and H_2O at 190 K – Atmospheric applications, *Atmos. Chem. Phys.*, 3, 1779–1789, doi:10.5194/acp-3-1779-2003, 2003.

30816

30817

Table 1. Characteristic parameters of the used stirred flow reactor (SFR).

Reactor volume (upper chamber)	2036 cm ³
MS (lower) chamber	1750 cm ³
Reactor internal surface	1885 cm ²
HCl calibrated volume – inlet line	62 cm ³
H ₂ O calibrated volume – inlet line	44 cm ³
Si support area (one side)	A _{Si} = 0.99 cm ²
Reactor wall temperature	T _w = 315 K
Gas-surface collision frequency at 315 K, one side	7.39 s ⁻¹ (H ₂ O) 5.22 s ⁻¹ (HCl)
$\omega = \frac{\bar{c}}{4V} \cdot A_{\text{Si}} = \sqrt{\frac{8RT}{\pi M}} \cdot \frac{A_{\text{Si}}}{4V} \text{ s}^{-1}$ ^a	
Escape rate constant ^b	C _S = 0.0408 ± 0.0004 (small orifice) C _L = 0.161 ± 0.002 (large orifice) C _{S+L} = 0.194 ± 0.003 (small + large orifice)
$k_{\text{esc}}^{\text{SF}} = C \cdot \sqrt{\frac{T}{M}} \text{ s}^{-1}$	

^a M in kg; A_{Si} in m²; V in m³.

^b M in g.

30818

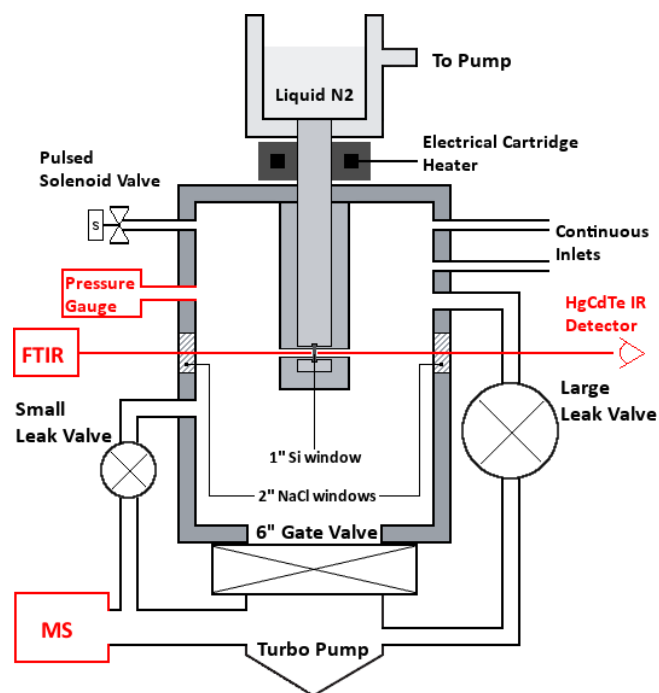


Fig. 1. Schematic drawing of the reactor used in this work. The diagnostic tools are highlighted in red and important parameters are listed in Table 1.

30821

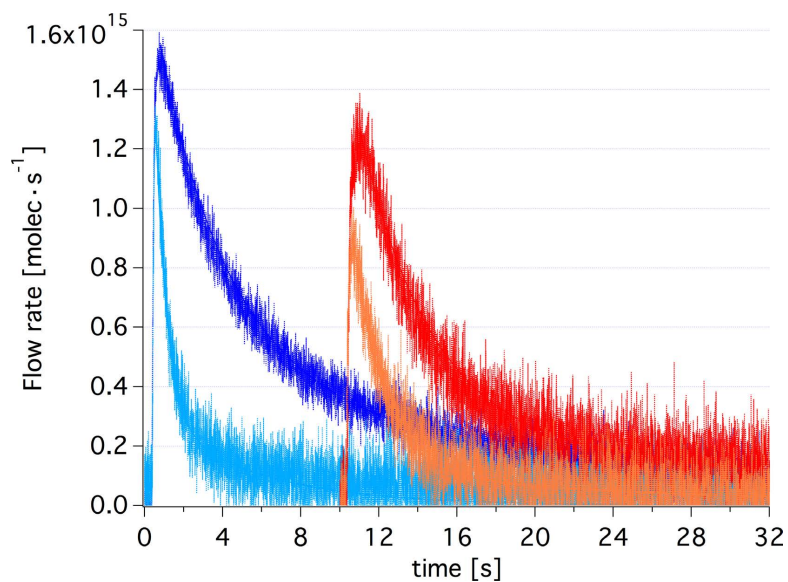


Fig. 2. Pulses of HCl and H₂O. The dark blue curve is a pulse of 1.5×10^{16} molecules of H₂O ($m/z = 18$) admitted into the reactor with the cryostat at $T_w = 315$ K for the measurement of uptake on the reactor walls. Likewise, the red curve is a pulse of 4.7×10^{16} molecules of HCl ($m/z = 36$) admitted into the reactor at $T_w = 315$ K. The light blue curve is a pulse of 2.7×10^{16} molecules of H₂O admitted in the presence of an HH film at 185 K, the orange curve is a pulse of 3.4×10^{16} molecules of HCl admitted in the presence of an HH film at 170 K. An offset of 10 s has been applied to the HCl curves for clarity.

30822

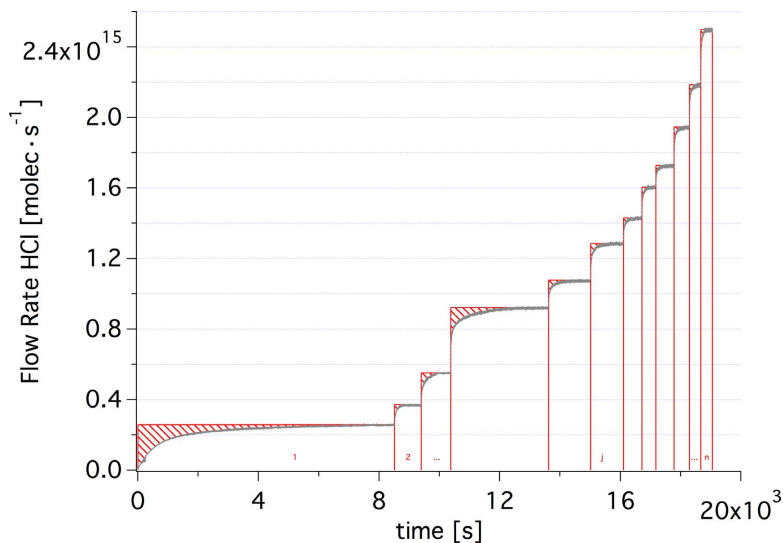


Fig. 3. Calibrated MS signal for the adsorption of HCl onto the stainless-steel reactor walls. The red shaded area represents the cumulative loss of molecules to the reactor walls at each j -th time interval as a function of the flow rate or partial HCl pressure.

30823

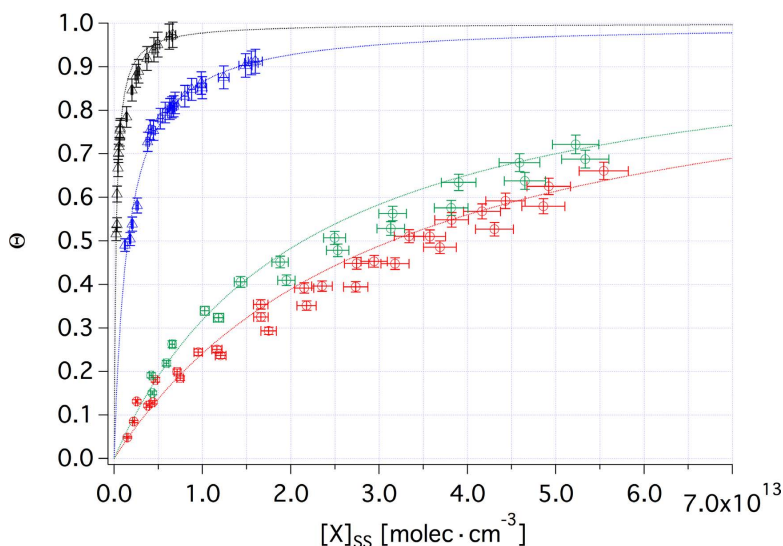


Fig. 4. Wall coverage as a function of HCl and H₂O concentration interacting with the reactor walls according to Langmuir using data of the type displayed in Fig. 3. The red symbols represent the interaction of pure H₂O and the green symbols the interaction of H₂O in the presence of an additional HCl flow $F_{in}(HCl) = 8 \times 10^{14} \text{ molec s}^{-1}$ admitted into the reactor. Similarly, the black symbols represent the interaction of pure HCl, the blue symbols the interaction of HCl in the presence of an additional H₂O flow $F_{in}(H_2O) = (3 \div 6) \times 10^{15} \text{ molec s}^{-1}$ admitted into the reactor. The parameters of the fitting curves may be found in Table 2.

30824

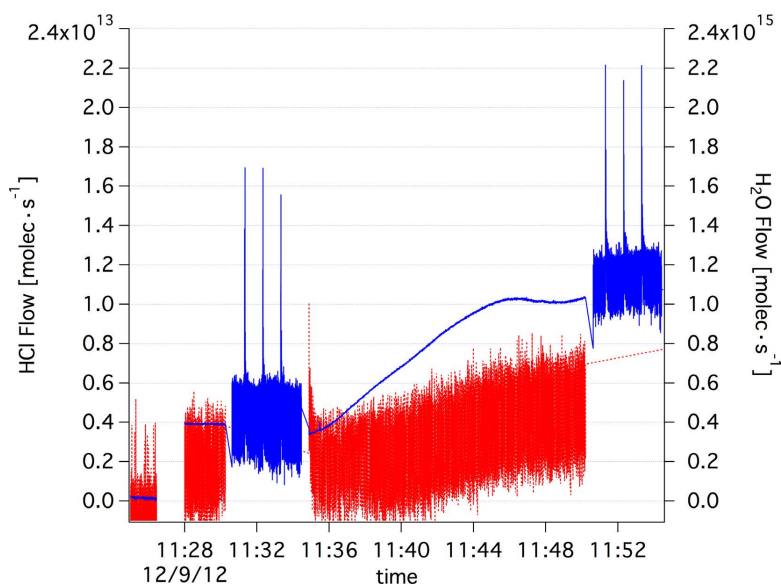


Fig. 5. PV and steady state experiment at low temperatures as a function of time on HH substrates. The blue curve (right axis) represents the H_2O flow rate with a series of pulses at 176 and 181.5K. The red curve (left axis) represents the corresponding HCl flow rate at the same temperatures. The flows of HCl and H_2O at background are reported at the beginning of the time series for comparison. Similar results are obtained when pulses of HCl are admitted in the reactor. An example of HCl pulses in the presence of ice is displayed in orange in Fig. 2 compared to HCl pulses (red curve) in the absence of ice.

30825

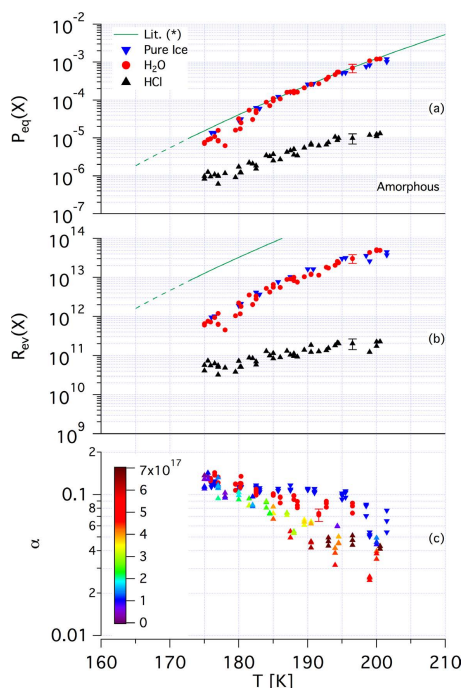


Fig. 6. Synopsis of kinetic results for amHCl using H_2O , HCl as a probe gas. The symbols used are explained in the text. The calculated relative error for α is 10%. The relative errors calculated for $R_{\text{eq}}(\text{HCl})$ and $P_{\text{eq}}(\text{HCl})$ are 30% whereas for $R_{\text{eq}}(\text{H}_2\text{O})$ and $P_{\text{eq}}(\text{H}_2\text{O})$ they are 25%. Examples of the amplitude of the errors are reported for selected points. The green line shows results from Marti and Mauersberger (1993). The colour scale shows the cumulative adsorbed dose after HCl pulsed gas admission.

30826

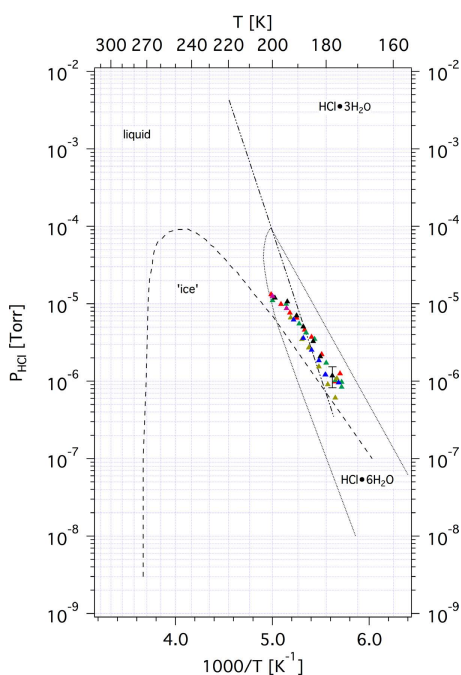


Fig. 7. Binary phase diagram of the HCl/H₂O system reconstructed from Molina and coworkers (Abbatt, 1992; Molina, 1994; Wooldridge, 1995). The full triangles represent calculated values of $P_{eq}(\text{HCl})$ for amHCl using the kinetic data of the present work. Different colours represent different experiment series.

30827

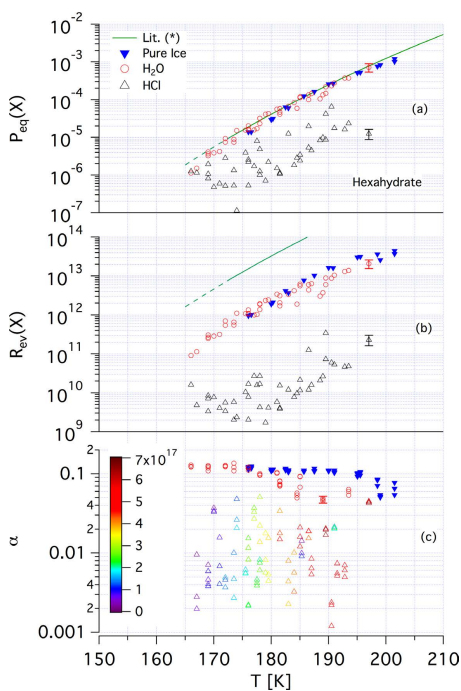


Fig. 8. Synopsis of kinetic results for HH using H₂O, HCl as a probe gas. The symbols used are explained in the text. The calculated relative error for α is 10 %. The relative errors calculated for $R_{ev}(\text{HCl})$ and $P_{eq}(\text{HCl})$ are 30 % whereas for $R_{ev}(\text{H}_2\text{O})$ and $P_{eq}(\text{H}_2\text{O})$ they are 25 %. Examples of the amplitude of the errors are reported for selected points. The green line shows results from Marti and Mauersberger (1993). The colour scale shows the cumulative adsorbed dose after HCl pulsed gas admission.

30828

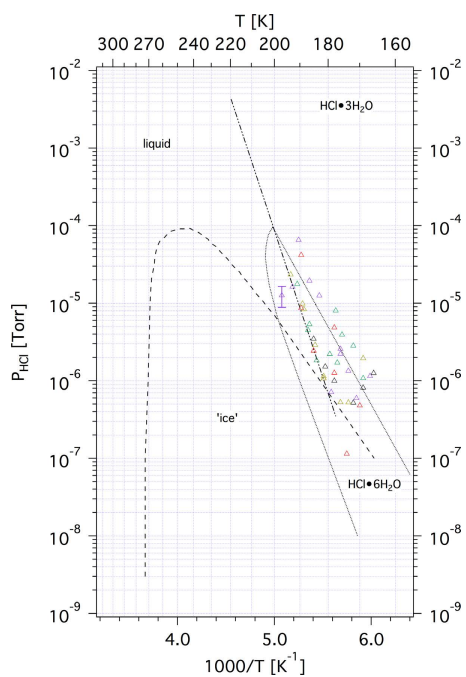


Fig. 9. Binary phase diagram of the HCl/H₂O system. The empty triangles represent calculated values of $P_{\text{eq}}(\text{HCl})$ for HH using the kinetic data for adsorption and desorption of the present work. Different colours represent different experiment series.

30829

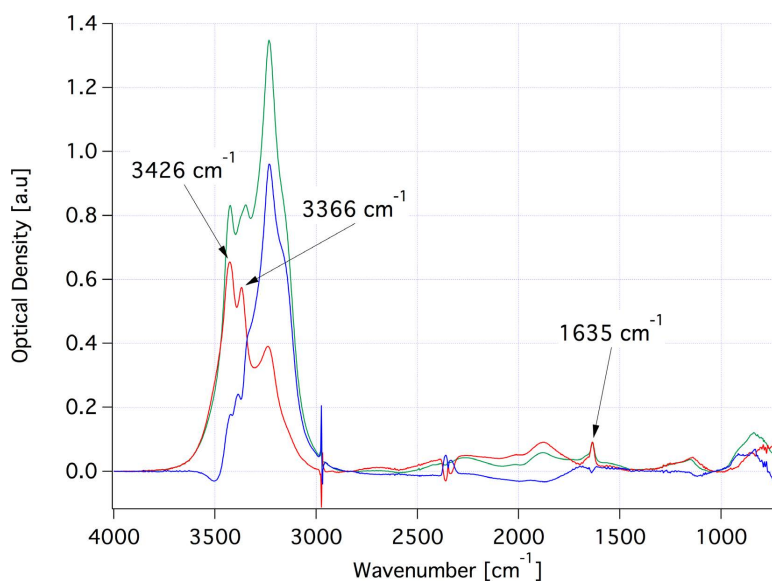


Fig. 10. Deconvolution of a measured FTIR absorption spectrum of a H₂O/HH mixture using its pure ice (blue) and pure HH (red) components. The measured composite FTIR absorption spectrum is shown in green.

30830

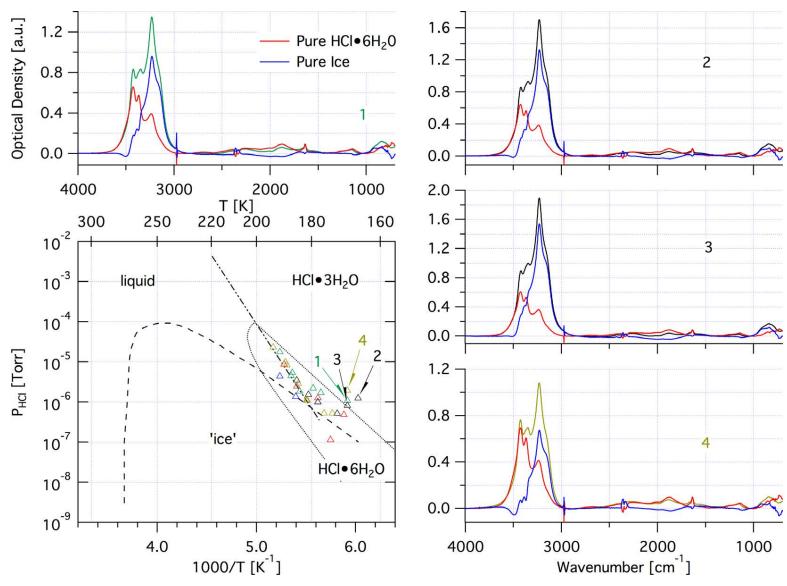


Fig. 11. Selected measured FTIR spectra with their deconvolution into pure ice (blue) and pure HH (red) component. The measured FTIR absorption spectra are coloured according to where they fit into the binary HCl/H₂O Phase Diagram.

30831

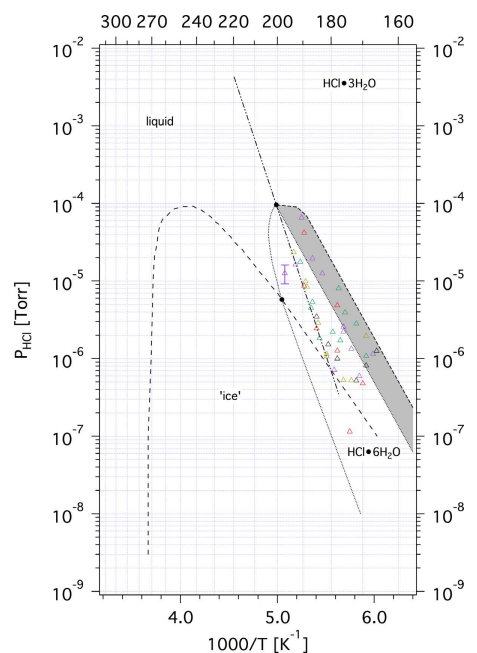


Fig. 12. Phase diagram of the HCl/H₂O system. The shaded area is the proposed extension of the HH existence area according to the results of the present work. The quadruple points (black dots) have been preserved.

30832

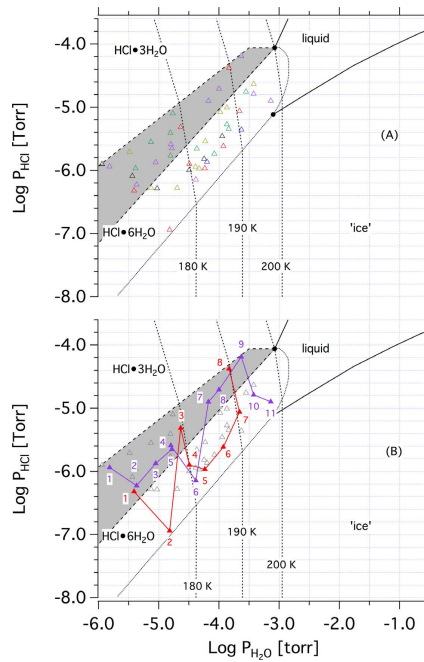


Fig. 13. Phase diagram of the HCl/H₂O system reconstructed from Hanson and Mauersberger, 1990. The empty coloured triangles represent calculated values of $P_{eq}(\text{HCl})$ and $P_{eq}(\text{H}_2\text{O})$ for HH using the kinetic results for adsorption and desorption of H₂O and HCl of the present work, according to Eq. (22). Different colours represent different experiment series. The shaded area is the proposed extension of the HH existence area according to the results of the present work with both quadruple points preserved. Panel (B) shows two different experiment series where the temporal evolution of the sample is discussed. Details may be found in the text.

30833

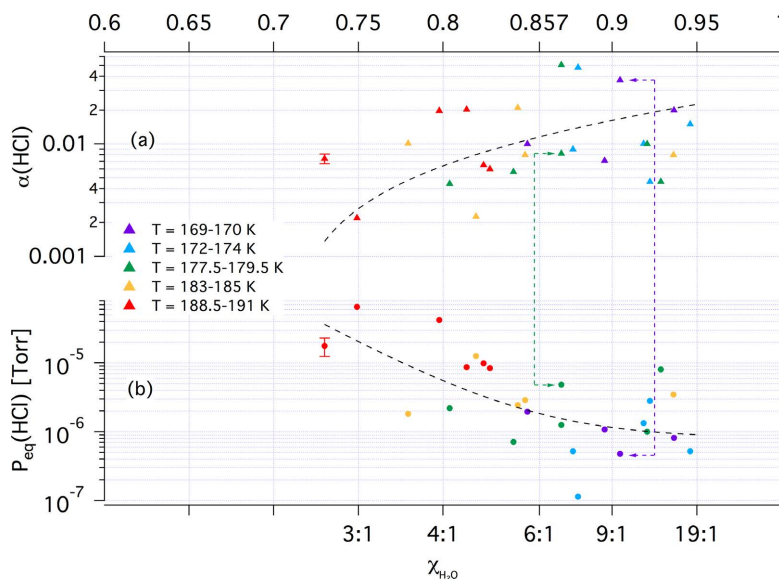


Fig. 14. $P_{eq}(\text{HCl})$ and $\alpha(\text{HCl})$ as a function of mole fraction of H₂O in HH film. The bottom and top axes indicate the H₂O : HCl ratio and the H₂O weight percentage in the film, respectively. Colours identify different temperature ranges and the broken lines just serve to guide the eye. Coloured arrows indicate an example of pairs of data points.

30834

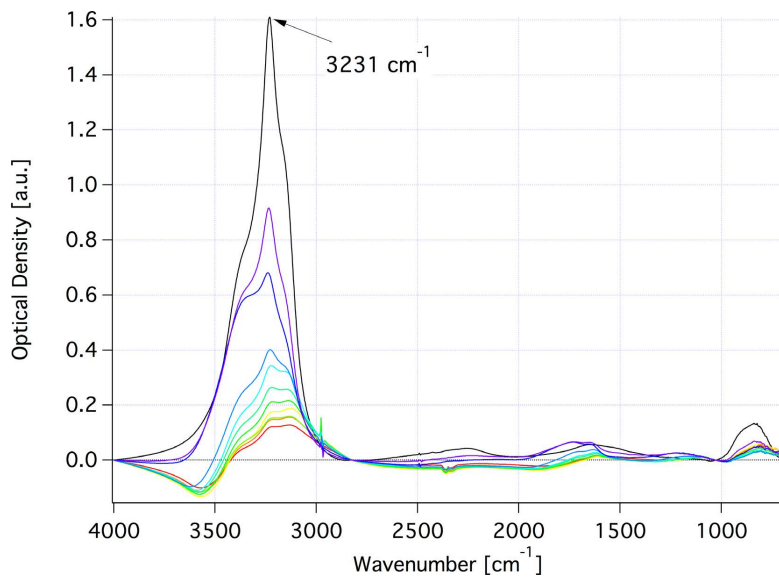


Fig. 15. Evolution of amHCl film. The spectrum of a pure ice film is represented in black and the conversion of an amHCl from a H₂O-rich film (purple spectrum) to an amorphous HCl/ice film (red spectrum) while pumping under SFR are displayed in colour. The spectra are colour-coded as a function of temperature in the range 175 to 200 K, with each spectrum corresponding to a temperature increase of roughly 3 K. All spectra from blue to red have been measured in the aftermath of the first pulse in a series of consecutive PV experiments.

30835

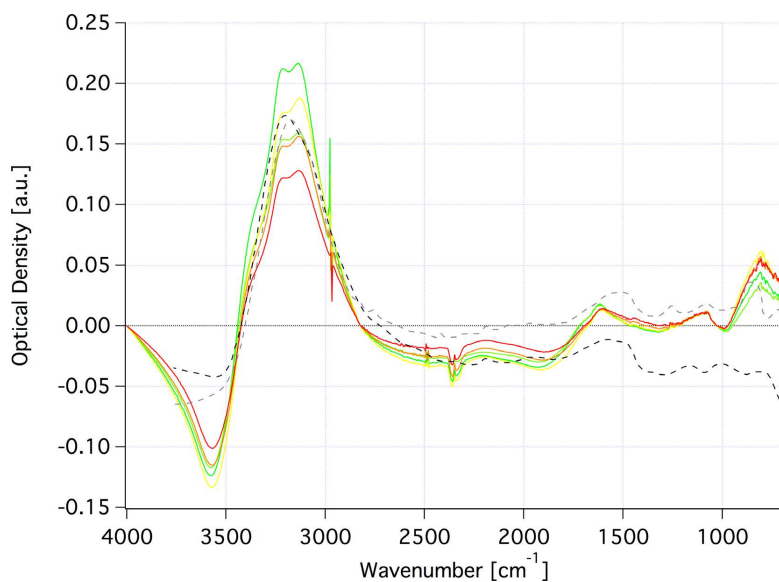


Fig. 16. Comparison of FTIR spectra of amHCl films. Our experimentally measured spectra are shown in colours according to temperature, whereas the dashed spectra correspond to samples made by condensing HCl : H₂O gaseous mixtures of ratios 1 : 200 (black line) and 1 : 50 (grey line) at 190 K of Xueref and Dominé (2003). The temperature of the ice sample ranges between 187 and 200 K with each spectrum measured in the aftermath of the first pulse in a series of PV experiments at temperature intervals of roughly 3 K.

30836

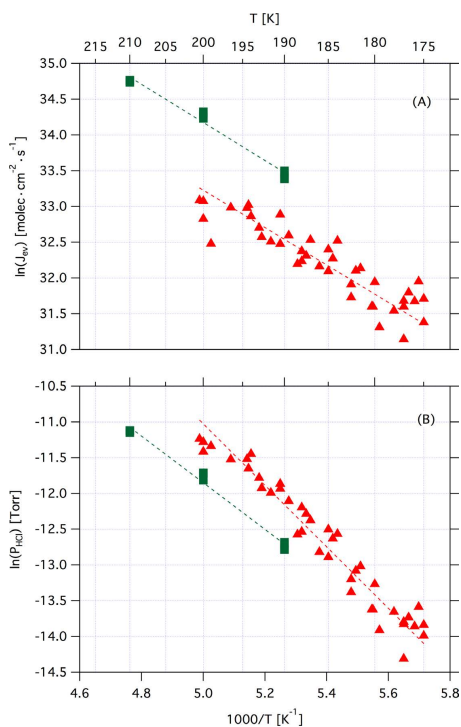


Fig. 17. Arrhenius plot of $J_{ev}(\text{HCl})$ (A) and van't Hoff plot of $P_{eq}(\text{HCl})$ (B). Red triangles represent the results for the interaction of HCl with amHCl/H₂O down to $T = 175$ K (this study) and green squares the results from a Knudsen flow reactor study addressing the HCl/H₂O liquid-ice coexistence region (Flückiger et al., 1998). The equations for the fitting lines may be found in the text.

30837

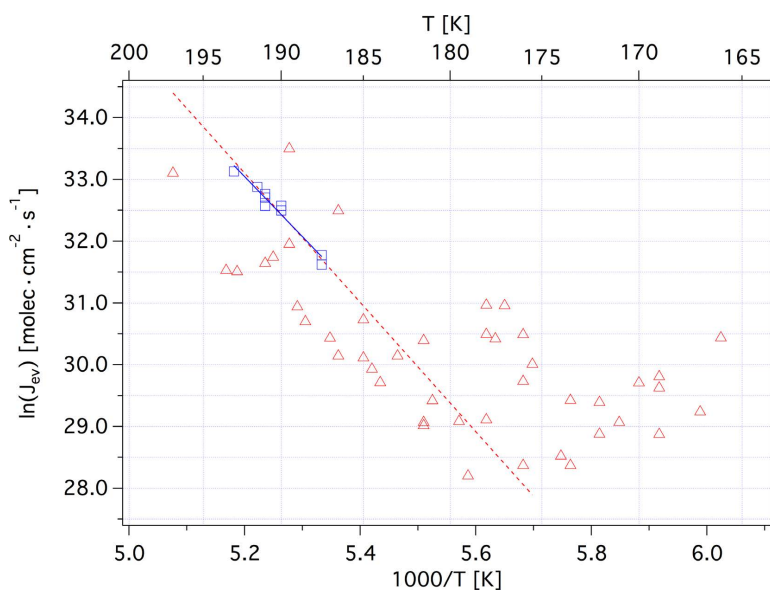


Fig. 18. Arrhenius plot of $J_{ev}(\text{HCl})$ for HCl·6H₂O. Red triangles represent the results of this study and blue squares the results of Chiesa and Rossi (2013) obtained from the decay of crystalline HCl·6H₂O. The equations for the linear fits may be found in the text.

30838

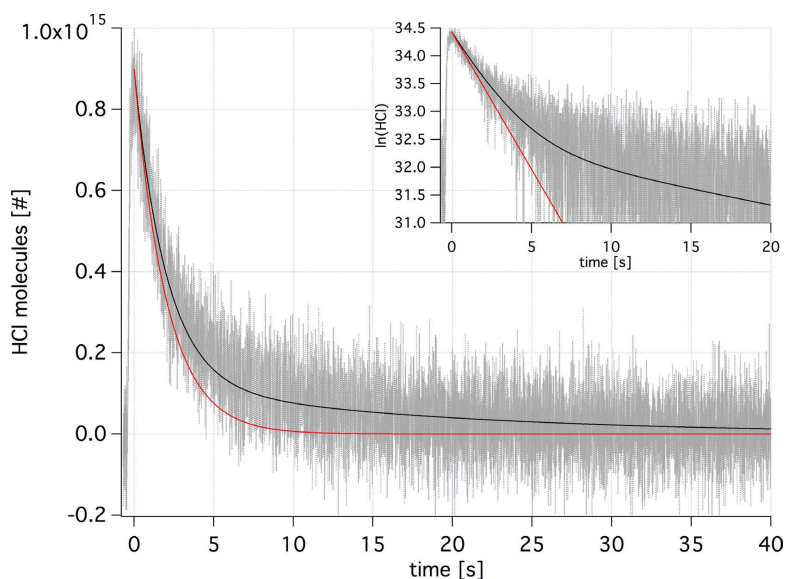


Fig. C1. Real time HCl PV experiment in the presence of ice at $T = 189.5$ K. The measured HCl calibrated signal is shown in grey as a function of time. In red and black fit curves of the signal. The red curve is calculated fitting the curve with an exponential decay whose constant is given by $k_d = k_{\text{esc}} + k_w + k_{\text{ice}}$. The black fit is calculated considering the signal decay as sum of a fast decay k_d and a slow desorption contribution from the walls and the ice. The insert shows the signal and the fits on a semi-logarithmic scale.